NGUYEN THI DUYEN

RESEARCH ON NAVIGATION SOLUTIONS FOR MOBILE ROBOTS IN AGRICULTURAL ENVIRONMENTAL AND CROP GROWTH MONITORING

SUMMARY OF DISSERTATION ON ELECTRICAL, ELECTRONICS AND TELECOMMUNICATION

Major: Control and Automation Engineering
Code: 9 52 02 16

Hanoi - 2026

The dissertation is completed at: Graduate University of Science and Technology, Vietnam Academy of Science and Technology

Supervisors:

Supervisor 1: Dr. Ngo Manh Tien, Institute of Physics, VAST

Supervisor 2: Prof. Dr. Phan Xuan Minh, International School, VNU

Referee 1: …

Referee 2: …

Referee 3: ….

The dissertation will be examined by Examination Board of Graduate   University of Science and Technology, Vietnam Academy of Science and Technology at……………………….. (time, date, year…)

INTRODUCTION

1. Rationale Of The Topic

The advancement of high-tech agriculture in the digital transformation era necessitates the robust integration of sensor systems, mobile robots, and artificial intelligence to automate monitoring, data acquisition, and analysis. Within this context, agricultural greenhouses serve as typical closed-environment cultivation systems that demand stringent control of environmental parameters—such as temperature, humidity, illumination, and nutrients—to ensure stable crop growth.

While the deployment of wireless sensor networks (WSNs) in greenhouses facilitates continuous monitoring of environmental parameters, it presents significant challenges regarding data acquisition coverage, energy constraints, and communication stability. Furthermore, plant growth monitoring and early pest and disease detection still rely heavily on manual observation, which is time-consuming and error-prone. Consequently, there is an urgent need for a more automated, efficient, and intelligent solution to enhance this process.

In this context, mobile robots (MRs) are considered ideal platforms for integration into agricultural monitoring systems. Leveraging their maneuverability, MRs can concurrently acquire environmental data from cluster heads (CHs) and capture crop images via imaging sensors positioned proximal to environmental nodes. However, to ensure system efficiency, it is imperative to develop navigation solutions that optimize robot trajectories, guaranteeing comprehensive data acquisition within the reporting threshold (ξ_0) while minimizing the energy consumption of sensor nodes within the wireless sensor network (WSN).

Concurrently, crop imagery acquired by mobile robots must undergo intelligent processing and analysis to facilitate growth monitoring and early pest and disease detection. Enhancing artificial intelligence models for image recognition will significantly boost the accuracy and efficacy of autonomous monitoring systems within practical greenhouse environments.

Based on the aforementioned analyses, the thesis title: "Navigation Solutions for Mobile Robots in Environmental and Crop Growth Monitoring" was selected to enhance the operational efficiency of mobile robots in agricultural production. Within this framework, the research focuses on developing navigation strategies for data acquisition from wireless sensor networks (WSNs) in greenhouses. Utilizing the collected crop imagery, the thesis proposes AI-driven solutions to improve monitoring quality, with an emphasis on early pest and disease detection.

The implementation of this research not only advances the development of intelligent mobile robotics in precision agriculture but also fosters the integrated application of control and automation technologies with artificial intelligence to manage, monitor, and optimize modern agricultural production

2. The Research Objectives And Tasks

- Mobile robot navigation in agricultural greenhouses ensures the comprehensive acquisition of measurement data from cluster heads (CHs) within the allowable reporting period, prioritizing the reduction of sensor node energy consumption in WSNs.

- AI-driven monitoring of crop growth facilitates early and accurate pest and disease detection, enabling timely preventive interventions to enhance overall yield and cultivation efficiency.

3. The Scientific and Practical Significances

- The Scientific Significance

The thesis investigates navigation solutions for mobile robots (MRs) to ensure comprehensive data acquisition from sensor nodes within the allowable reporting period while minimizing node energy consumption,,. Furthermore, it proposes enhanced artificial intelligence models to improve the quality of crop monitoring,. These scientific contributions establish a theoretical foundation for future research in intelligent agricultural robotics and advanced monitoring technologies

- The Practical Significance

The thesis holds practical significance by integrating mobile robotics and automation technology into agricultural greenhouse models. The mobile robot system concurrently performs environmental monitoring, crop growth tracking, and early pest and disease detection. The proposed navigation solutions facilitate comprehensive sensor data acquisition, optimize energy efficiency, and enhance monitoring performance. Furthermore, early and accurate detection enables timely interventions, reducing pesticide usage and mitigating environmental impacts. Ultimately, these research findings contribute to increased yields, improved product quality, and the promotion of clean, sustainable agriculture.

4. The Contributions Of The Study

- Proposing a navigation solution for mobile robots (MRs) to ensure comprehensive data acquisition from wireless sensor networks (WSNs) within the allowable reporting period, facilitating environmental and crop growth monitoring while minimizing the energy consumption of sensor nodes.

- Proposing an enhanced YOLO model to improve the detection quality of crop pests and diseases in agricultural greenhouses.

5. The Structure Of The Study

The thesis comprises an introduction and three main chapters. Chapter 1 provides a comprehensive literature review of related domestic and international research, identifies existing limitations, and defines the research tasks. Chapters 2 and 3 constitute the primary contributions of the work, focusing on navigation solutions for mobile robots and enhanced AI models for crop monitoring. The conclusion summarizes the key findings and outlines future research directions. Finally, the list of the candidate's publications and references are presented.

Chapter 1. LITERATURE REVIEW AND THEORETICAL BASIS OF MOBILE ROBOTS IN AGRICULTURAL GREENHOUSES

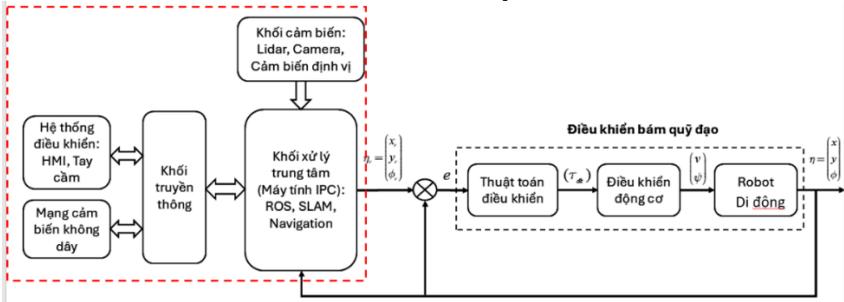## 1.1 The Architecture of the Mobile Robot Control System

Figure 1.1 The Architecture of the Mobile Robot Control System

1.2 The International and Domestic Research

Large-scale greenhouses (exceeding $10,000m^2$) necessitate intensive supervision, driving the adoption of high-tech solutions such as Wireless Sensor Networks (WSNs), robotic systems, and automated irrigation. This field has garnered significant interest from both domestic and international researchers. Specifically, studies proposed advanced IoT, AI, and computer vision solutions for greenhouse monitoring and control, while research developed microclimate monitoring systems by integrating autonomous robots with WSNs to enhance operational efficiency. However, these studies primarily focus on signal acquisition from sensor nodes for task execution, neglecting navigation strategies within WSNs to optimize network energy consumption and data collection efficiency. Meanwhile, other works developed mobile robots for greenhouse data collection but relied on fixed trajectories rather than adaptive navigation. Furthermore, although path-planning algorithms were proposed in, they were confined to small-scale environments and lacked integration with WSNs or specific sensor data acquisition tasks. Consequently, crop growth monitoring remains a prominent research focus.

1.3 Mobile Robotic Systems for Environmental and Crop Monitoring in Smart Greenhouses

Greenhouses spanning several thousand to tens of thousands of square meters are equipped with mobile robots and environmental/imaging sensors integrated into a Wireless Sensor Network (WSN) to monitor microclimate conditions and crop growth processes [Figure 1.2].

Figure 1.2 Agricultural greenhouse model for tomato cultivation across several hectares.

*** The Energy model of sensor nodes in Wireless Sensor Networks**

Sensor node energy consumption comprises the energy required for data transmission, data reception, and data processing [43].

The sensor node energy consumption for data transmission:

$$E_T(\gamma) = E_{elec}.\gamma + E_{amp}.d^\chi.\gamma \tag{1.1}$$

The sensor node energy consumption for data reception:

$$E_R(\gamma) = E_{elec}.\gamma \tag{1.2}$$

The sensor node energy consumption for data analysis:

$$E_{cpu}(\gamma) = E_{cpu}.\gamma \tag{1.3}$$

While: γ- the data packet length (bits)

d- the transmission distance (m)

E_{elec} – Transceiver circuitry energy consumption (nJ/bit)

E_{amp}- The signal amplification energy (nJ/bit/m²)

E_{cpu}- The energy consumption for data analysis (nJ/bit)

χ- The path loss exponent

The total energy consumption of the kth sensor node:

$$E_k(t) = E_T(\gamma) + E_R(\gamma) + E_{cpu}(\gamma) = \gamma(2E_{elec} + E_{cpu} + E_{amp}.d^\chi) \tag{1.4}$$

Consequently, the energy consumption of a sensor node is proportional to the packet size γ and the transmission distance. Given identical packet sizes, energy consumption increases as the transmission distance grows.

This thesis focuses on utilizing mobile robots (MRs) to collect data from cluster heads (CHs) to shorten signal transmission distances, thereby conserving sensor node energy. To address this, the MR navigates to designated sensor nodes to gather greenhouse cultivation data. Subsequently, the robot returns to the Network Control Center (NCC) to transmit the collected data for processing and supervisory control decision-making.

The integrating mobile robots for crop image acquisition via fixed cameras with data preprocessing and AI-driven growth monitoring represents an essential trend in smart agriculture. This research direction not only improves monitoring quality and early pest detection but also optimizes operational costs, accuracy, and automation in greenhouse management.

The effectiveness of mobile robots in agricultural environmental and crop growth monitoring is contingent upon the rationality of their movement within the monitoring environment. Developing appropriate navigation solutions is essential to ensuring optimal mobile robot operation in these settings.

1.4 The conclusion of chapter 1

Chapter 1 presents an overview of domestic and international research related to the operation of mobile robots for environmental monitoring and crop growth assessment in agriculture, with emphasis on greenhouse environments, mobile robot navigation, and artificial intelligence applications. Based on this review, the dissertation identifies the following research objectives: to investigate and develop navigation strategies for a mobile robot tasked with collecting environmental data and crop images from cluster-head sensor

nodes within a wireless sensor network for agricultural environmental and crop growth monitoring. Furthermore, the dissertation addresses a second problem, namely monitoring crop development in agricultural greenhouses, with priority given to AI-based detection of plant diseases and pests. The detailed contents of these objectives are presented in the subsequent chapters of the dissertation.

Chapter 2. A NAVIGATION STRATEGY FOR MOBILE ROBOT IN AGRICULTURAL MONITORING DATA ACQUISITION

A mobile robot tasked with collecting greenhouse environmental data from a wireless sensor network is essential for environmental and crop monitoring in agriculture. The efficiency of data acquisition from the wireless sensor network depends significantly on the robot's mobility performance. In this chapter, the dissertation first investigates the wireless sensor network system deployed in an agricultural greenhouse. It then studies and proposes a navigation strategy for the mobile robot to ensure timely acquisition of environmental parameters and crop images within a predefined time horizon, while prioritizing energy efficiency of cluster-head sensor nodes. The chapter concludes with a summary of the main findings.

2.1 The Wireless sensor network model in agricultural greenhouse

In large-scale agricultural greenhouses with an area of several hectares or more, cultivation zones are typically divided into multiple sections; accordingly, multiple sensor clusters are deployed in each zone. Each cluster includes a Cluster Head (CH) that collects data from local sensor nodes. The Cluster Head (CH) serves as the central node of a sensor cluster, responsible for aggregating data from local sensor nodes, performing preliminary processing, and transmitting the data to the base station; it is also referred to as the cluster coordinator. The wireless sensor network comprises approximately 200–250 sensor nodes uniformly distributed at different locations to ensure full coverage of the greenhouse (Fig. 2.1).
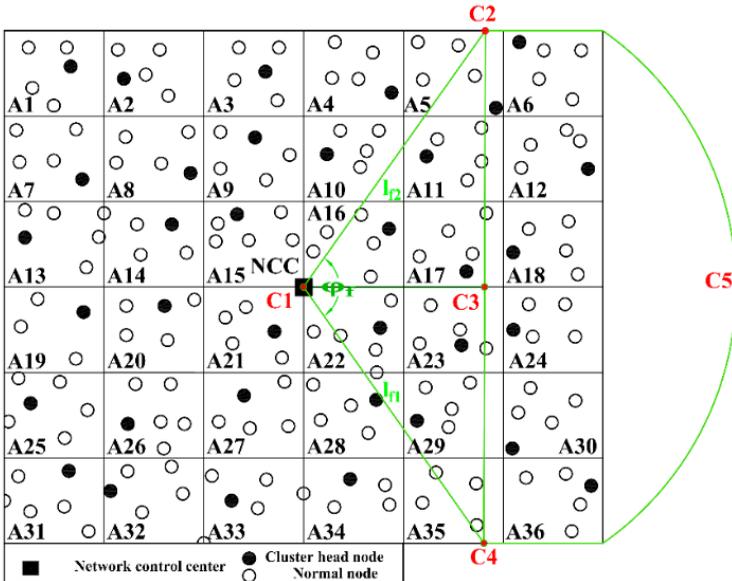

Figure 2.1 The Wireless sensor network model

2.2 The number of Cluster head nodes determination

The wireless sensor network model with a rectangular sensing field is illustrated in Fig. 2.1.
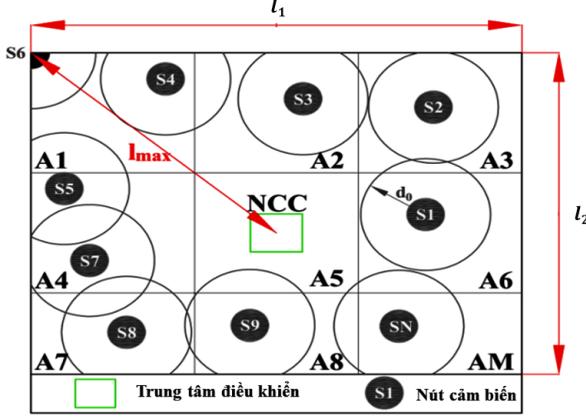

Figure 2.2 The number of Cluster head nodes (CH) determination

If the number of cluster heads (CHs) is too small, each CH must handle a large volume of data from numerous local sensor nodes and transmit over longer distances, resulting in high energy consumption. Conversely, if the number of CHs is excessive, the mobile robot must visit more locations for data collection, which may prevent complete data acquisition within the allowable time.

To address this issue, the dissertation determines an appropriate number of cluster head nodes to minimize energy consumption at sensor nodes while ensuring data collection is completed within a predefined time constraint.

Consider a rectangular wireless sensor network as illustrated in Fig. 2.5, where l_1, and l_2 denote the length and width of the sensing field, respectively. During the initial deployment phase, each sensor node has an identical communication range with transmission radius $R_t=d_0$. The network coordination center (NCC) is located at the center of the sensing field. To determine the optimal number of cluster head nodes—equivalent to the number of sensor clusters—by partitioning the sensing field into M equal regions, the following theorem is stated:

Theorem 1: Let l_{max} denote the maximum distance between the NCC and a sensor node within the considered sensing field; R the data transmission rate between the cluster head (CH) and the mobile robot (MR); and v prescribed the velocity of the MR. An appropriate partitioning of the sensing field into M equal regions exists if the following condition is satisfied:

$$M \geq \frac{\gamma l_1 l_2 v}{\pi l_0^2 R \left(\xi_0 v - 2 l_{max} \right)} \tag{2.1}$$

2.3 Proposed navigation algorithm for data collection of mobile Robot

The mobile robot (MR) navigation problem is formulated such that the MR departs from the NCC, visits cluster head nodes to collect data, and subsequently returns to the NCC to upload the acquired data.

The MR trajectory is constructed based on a geometric heuristic solution [33], which provides an approximate solution to the Travelling Salesman Problem (TSP). This approach exploits the geometric properties of nodes in wireless sensor networks (WSNs) to obtain a near-optimal path with low computational cost, thereby enabling the generation of a short traversal route.

The MR is required to collect complete data from N nodes in the network within a predefined operational time horizon ξ_0, while minimizing energy consumption at the sensor nodes.

To satisfy these requirements, the following theorem is stated:

Theorem 2: Let $\mathcal{R}_f(t)$ denote the total path length of the mobile robot (MR) within its operational area during the t-th round. To collect all sensor data from N_f sensor nodes within the reporting time threshold ξ_0, the MR must travel at a velocity $v(t)$, while data are acquired at each cluster head (CH) with transmission rate R. An algorithm is considered effective for data collection without sensor data loss if and only if the following condition is satisfied:

$$\left(\frac{\mathcal{R}_f(t)}{v(t)} + \frac{\gamma N_f}{R}\right) \leq \xi_0 \tag{2.2}$$

The trajectory of the mobile robot through the cluster head nodes within the assigned sensing region, ensuring data collection within the allowable time, is constructed based on a geometric heuristic approach and illustrated in Fig. 2.3.
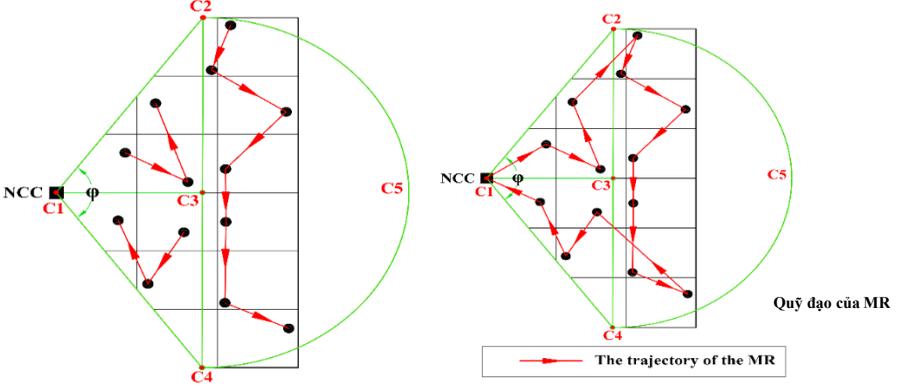
Hình 2.3 The MR trajectory based on the Heuristic method

The total path length of MR_f depends not only on the sector angle φ_f, $f \in \{1, \dots, F\}$, the number of cluster heads (CHs) to be visited, and the total number of sensor nodes within the assigned region of MR_f, but also on the geographical distribution of the CHs. Therefore, according to the time threshold ξ_0, the sector angle φ_f is adjusted such that each cluster head within the circular sector is visited within the reporting period under the following condition:

$$\varphi_f \leq \frac{2R}{\gamma \rho l_f^2}\left(\xi_0 - \frac{2l_f}{v(t)}\right) \tag{2.3}$$

Accordingly, the objective function is formulated as follows:

$$min\left\{\sum_{i=0}^{N}\sum_{j=0}^{N}\sum_{i \neq j, f=1}^{N} \xi_{ij}\, x_{ij}\right\} \tag{2.4}$$

Subject to the following constraints:

$$\sum_{i=1}^{N} x_{ij} = 1 \; v\acute{o}i \; j = 0$$

$$\sum_{j=1}^{N} x_{ij} = 1 \; v\acute{o}i \; i = 0$$

$$\sum_{i=0}^{N} \sum_{j=0, i \neq j}^{N} \xi_{ij} x_{ij} \leq \xi_0,$$

where N denotes the total number of sensor nodes in the WSN; ξ_{ij} represents the time required for data transmission and for the MR to travel from node i to node j.

The navigation process of the mobile robot for collecting sensor data from cluster heads in the wireless sensor network is illustrated in Fig. 2.4.

Navigation Algorithm for a Mobile Robot to Collect Data from a Wireless Sensor Network (MRNA - Monitoring Robot Navigation Algorithm) is given as follows:

***Input*:** Parameters of model: Number of sensor nodes N, Network size l_1 x l_2; The velocity of the mobile robot (v); Initial energy E_0; Threshold of reporting time ξ_0; data packet γ-bit; Node density (ρ); Transmission range (R).

***Output*:**
- The number of optimal subareas M;
- Assignment area to collect data for each MR φ_f;
- The optimal trajectory of each MR at each operation round $\Re_f(t)$.

1: Estimate the number of cluster (*M*) for energy efficient deployment scheme in WSNs based on equation (2.1).

2: Estimate the assignment area (2.3) for each MR and then calculating the number of MRs need to be utilized for data collection. Steps 3 and 4 will be done by the NCC. After these steps, the NCC will flood this information to all sensor nodes in the sensing field. By this way, every sensor node know its cluster and the MR's assignment area, where it belongs to. Then every sensor nodes in each cluster will elected their cluster head node. The locations of these cluster head nodes will be sent back to the NCC for finding the optimal trajectories of *F* mobile robots.

3: Begin the trajectory of the *MRf* starting from the NCC (the depot) $\Re^i_f=0$.

4: Among all unvisited CHs inside the assignment area of *MRf* select the farthest CH from the NCC and add into the current trajectory of the *MRf*: $\Re^i_f=1$.

5: If all CHs are visited, then goto step 7.
Else: Go to step 6.

6: Find the best candidate node among unvisited CHs, which the *MRf* comes to visit with the smallest spending time based on Equation (2.4). Update the reporting time $\xi(t)$ of MR. Go back to step 5.

7: The algorithm terminates with a mobile robot trajectory that satisfies the requirements for complete sensor data acquisition.
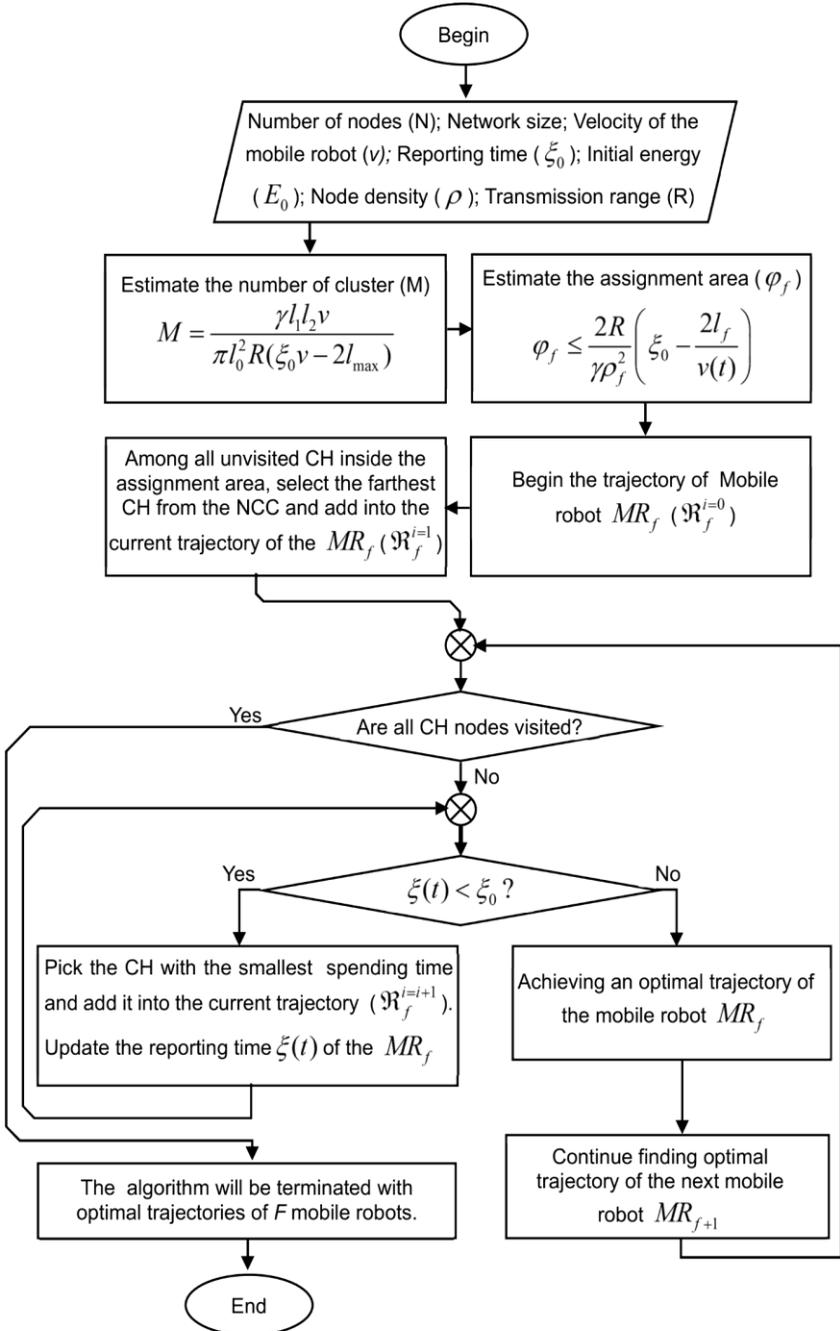
Hình 2.4 The flowchart of the proposed MRNA algorithm

2.4 Numerical results and discussion

The dissertation conducts simulations under two scenarios: a wireless sensor network of 150×150m containing 200 sensor nodes, and a network of 200×200m comprising 250 sensor nodes. The simulation results of the proposed algorithm are obtained using the MATLAB environment. The simulation parameters are listed in Table 2.1.

Table 2.1. The settings of simulation parameters

Parameter	Value
Node deployment	Uniform
The initial energy (E_0)	0.1 (J)
Energy for data aggregation (E_{DA})	5 (nJ/bit)
Energy consumption E_{elec}	50 (nJ/bit)
ε_{fs}	10 (pJ/bit/m^2)
ε_{mp}	0.0013 (pJ/bit/m^4)
Data packet length (γ)	4000 (bits)
Transmission range (R_t)	30 (m)
Data transmission rate (R)	250 (Kb/s)
Reporting time (ξ_0)	60 (s)

The simulation results presented in Table 2.2 indicate that, in all experimental cases, each mobile robot follows the shortest path to collect all sensor data within its assigned region during the reporting period.

The dissertation performs simulations to compare the proposed MRNA algorithm with OMS1, OMS2 [16], and the Routing Algorithm [17] in order to evaluate the lifetime of the wireless sensor network when the mobile robot is navigated using MRNA. The results are presented in Table 2.3 and Fig. 2.5.

Based on the results obtained from 350 experimental trials, the maximum network lifetime achieved using the OMS2 algorithm is 2,964 rounds [16]. In contrast, the proposed MRNA algorithm consistently outperforms OMS2 under identical experimental conditions, attaining an average maximum network lifetime of 3,125 rounds. Accordingly, the application of the MRNA algorithm improves the WSN lifetime by approximately 5.4% compared to OMS2.
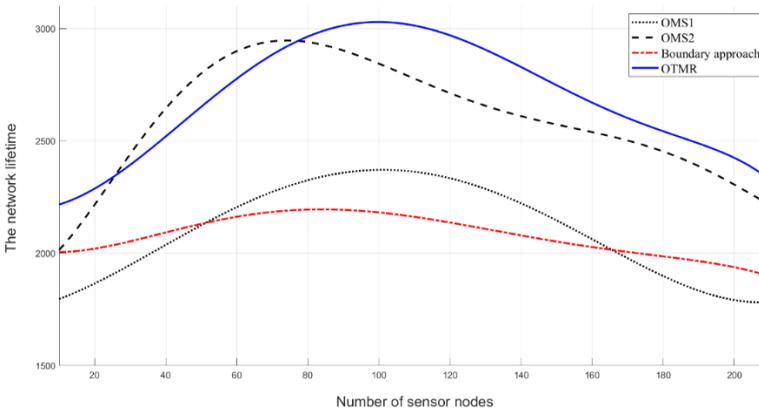

Figure 2.5 The comparison of the network lifetime

Table 2.2. The MR trajectory length and execution time

No.	Network size		N	ξ_0	v (m/s)	The MR trajectory length (m)	The execution time ξ (s)
	l_1 (m)	l_2 (m)					
1	200	200	250	60	3,0	397,5	58,1
2	200	200	250	60	3,0	395,4	56,6
3	200	200	250	60	3,0	391,5	54,0
4	200	200	250	60	3,0	389,4	52,6
5	200	200	250	60	3,0	399,3	59,3
6	200	200	250	60	3,0	399,6	59,5
7	200	200	250	60	3,0	391,8	54,2
8	200	200	250	60	3,0	395,1	56,4
9	200	200	250	60	3,0	396,6	57,5
10	200	200	250	60	3,0	394,8	56,2
11	150	150	200	60	2,0	348,1	49,5
12	150	150	200	60	2,0	349,6	51,1
13	150	150	200	60	2,0	350,0	51,5
14	150	150	200	60	2,0	347,9	49,3
15	150	150	200	60	2,0	348,6	50,0
16	150	150	200	60	2,0	348,2	49,6
17	150	150	200	60	2,0	349,3	50,8
18	150	150	200	60	2,0	348,6	50,0
19	150	150	200	60	2,0	348,3	49,7
20	150	150	200	60	2,0	349,7	51,2

Table 2.3. Network lifetime under varying the network sizes and the network densities

No.	Network size		N	R_t (m)	Network lifetime
	l_1 (m)	L_2 (m)			
1	200	200	250	10	3417
2				15	3364
3				20	3311
4				25	3258
5				30	3125
6				35	3056
7				40	2542
8				45	2318
9				50	1872
10				55	1561
11	150	150	200	10	3381
12				15	3325
13				20	3247
14				25	3115
15				30	3057
16				35	2465
17				40	2084
18				45	1912
19				50	1815
20				55	1673

2.5 The conclusion of chapter 2

In Chapter 2, the dissertation partitions the sensing field into sensor clusters and determines the appropriate number of cluster head nodes to be visited by the mobile robot within the assigned region to ensure data collection within the allowable time while minimizing energy consumption at sensor nodes. A navigation algorithm is then proposed to guarantee complete sensor data acquisition within the specified time constraint. Simulation results and comparisons with related algorithms demonstrate the effectiveness of the proposed approach. The findings of this chapter have been published in Publication No. 4 of the doctoral candidate.

Chapter 3. ENHANCING THE QUALITY OF CROP PEST DISEASE DETECTION BASED ON ARTIFICIAL INTELLIGENCE

3.1 Introduction

In modern agricultural greenhouse systems, monitoring crop development is a critical task to ensure productivity and product quality. In addition to collecting environmental data from wireless sensor networks, direct observation of crop conditions through imaging provides more detailed and intuitive information. To this end, a mobile robot is deployed to navigate to designated monitoring areas, where onboard cameras capture crop images and transmit the data to the robot for delivery to the control center for processing.

However, a major challenge lies in developing effective image-processing methods capable of accurately detecting plant growth status, nutritional conditions, and signs of pests and diseases. Conventional image-processing techniques often encounter limitations in complex greenhouse environments characterized by varying illumination, high planting density, and morphological changes across growth stages. Therefore, the adoption of advanced data-processing approaches combined with improved artificial intelligence models is necessary to enhance detection accuracy and practical applicability.

In particular, prioritizing the detection and monitoring of crop pests and diseases enables timely intervention, minimizes losses, and optimizes production efficiency. In this chapter, the dissertation focuses on image-based crop growth monitoring and proposes enhancements to artificial intelligence models to meet the practical requirements of intelligent greenhouse systems.
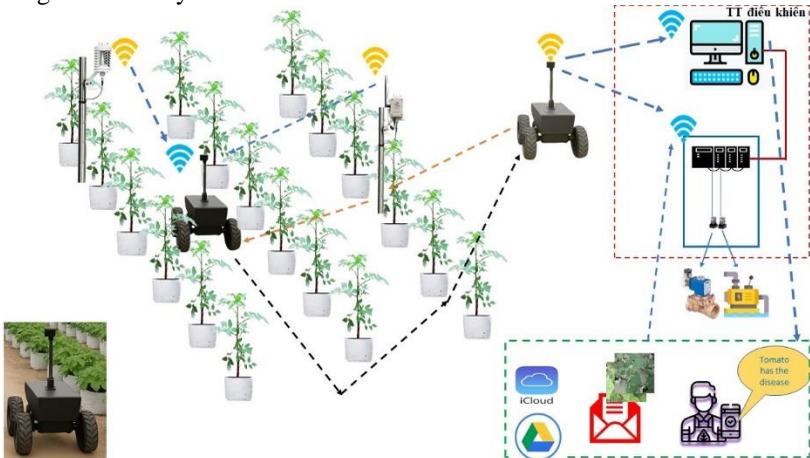

Figure 3.1 Mobile Robot model for sensor data acquisition and crop monitoring

3.2 Denoising crop images acquired by the Mobile Robot at image sensor nodes
Selection of the Threshold Function

- The selection of the threshold function determines the estimation strategy applied to the wavelet coefficients during the denoising process.

- Among commonly used approaches, the two principal thresholding functions in wavelet-based denoising [64] are:

- Hard Thresholding function.
- Soft Thresholding function.

These two methods differ in their treatment of wavelet coefficients below the threshold, thereby directly affecting noise suppression performance and the preservation of image details.

The hard-thresholding function is defined by Equation (3.1).

$$\widehat{w}_{i,j} = \begin{cases} w_{ij}, & \text{nếu } w_{ij} > \lambda \\ 0, & \text{ngược lại} \end{cases} \tag{3.1}$$

The soft-thresholding function is defined by the following expression: (3.2)

$$\widehat{w}_{i,j} = \begin{cases} w_{ij} - \lambda & \text{nếu } w_{ij} > \lambda \\ w_{ij} + \lambda & \text{nếu } w_{ij} < -\lambda \\ 0, & \text{ngược lại} \end{cases} \tag{3.2}$$

Where: w_{ij} denotes the original wavelet coefficient, $\widehat{w}_{i,j}$ is the wavelet coefficient after applying the thresholding function., và λ is threshold value.

Hard and soft thresholding function $\widehat{w}_{i,j}$ are illustrated in Figs. 3.2(a) and 3.2(b), respectively.

Dual-threshold shrinkage function- DuTS:

To mitigate pseudo-Gibbs artifacts introduced by conventional thresholding functions, the DuTS function was proposed in [65].

The main idea of this approach is as follows:

- Preserve coefficients with large magnitudes;
- Completely eliminate coefficients with very small magnitudes;

- For coefficients lying between the two threshold values λ_1, λ_2, a piecewise linear attenuation function is applied, whereby smaller coefficients within this interval are attenuated more strongly.

The proposed thresholding function based on the DuTS method is expressed in Equations (3.3) and (3.4).

$$\widehat{w}_{i,j}(\lambda_1, \lambda_2) = \begin{cases} w_{ij} & \text{nếu } |w_{ij}| > \lambda_2 \\ sign(w_{ij})A(w_{ij}) & \text{nếu } \lambda_1 < |w_{ij}| < \lambda_2 \\ 0, & \text{ngược lại} \end{cases} \tag{3.3}$$

$$A(w_{i,j}) = \frac{\lambda_1 \lambda_2 \left(|w_{i,j}| - \lambda_1 \right)}{\lambda_2 - \lambda_1} \tag{3.4}$$

Where: $sign(w_{i,j})$ is denotes the sign of the wavelet coefficient $w_{i,j}$. $\lambda_2 = \kappa \lambda_1, \kappa \in \cancel{C}$ and $\kappa \neq 1$. The DuTS function $\widehat{w}(\lambda_1, \lambda_2)$ is illustrated in the corresponding figure 3.2.c.
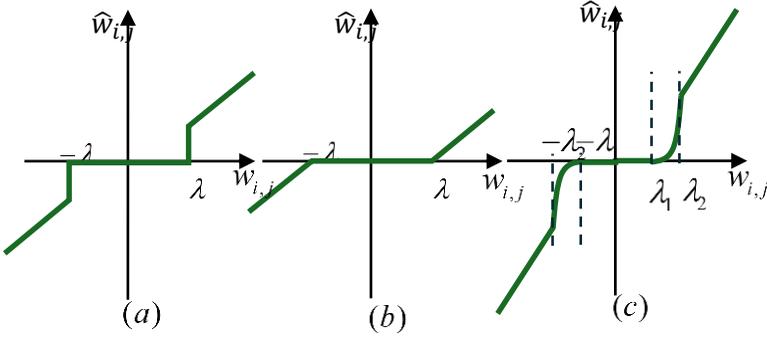
Figure 3.2 The thresholding functions are applied to the wavelet coefficients.

- ***Determination of the appropriate threshold value***

BayesShrink Threshold:

Based on the statistical characteristics of wavelet coefficients in natural images, Chang et al. [66] proposed the BayesShrink threshold estimation method.

This approach assumes that the noise-free wavelet coefficients follow a Generalized Gaussian Distribution (GGD). Experimental studies indicate that, except for the LL subband, most wavelet coefficients in natural images exhibit a symmetric distribution around zero with a sharp peak at the origin. Therefore, they can be effectively modeled by a zero-mean GGD.

The BayesShrink threshold is derived within a Bayesian framework to achieve optimal denoising performance under this assumption. Specifically, assuming that the wavelet coefficients follow a Generalized Gaussian Distribution, the optimal threshold can be obtained according to the Bayesian estimation criterion and is expressed as follows:

$$\lambda = \frac{\hat{\sigma}_w^2}{\hat{\sigma}_x} \tag{3.5}$$

Where: $\hat{\sigma}_w$ is determined in the following equation:

$$\hat{\sigma}_w = \frac{\text{Median}\left(\left|C_{i,j}\right|\right)}{0.6745}, \qquad C_{i,j} \in HH^1 \tag{3.6}$$ and $\hat{\sigma}_x$ represents the estimated

value derived from the wavelet coefficients in each subband. The value of $\hat{\sigma}_x$ is computed by Equations (3.7) and (3.8).

$$\hat{\sigma}_x = \sqrt{\max\left(\hat{\sigma}_y^2 - \hat{\sigma}_w^2, 0\right)} \tag{3.7}$$

$$\hat{\sigma}_y = \frac{1}{n^2} \sum_{j,k=1}^{n} C_{j,k}^2 \tag{3.8}$$

Proposing the threshold estimation method based on the BayesShrink approach

As presented in Equations (3.5) and (3.7), the appropriate threshold based on the Bayesian estimation principle is determined in Eq. (3.9):

$$\lambda = \frac{\hat{\sigma}_w^2}{\hat{\sigma}_x} = \frac{\hat{\sigma}_w^2}{\sqrt{\max\left(\hat{\sigma}_y^2 - \hat{\sigma}_w^2, 0\right)}} \qquad (3.9)$$

If $\hat{\sigma}_y^2 \le \hat{\sigma}_w^2$ then $\hat{\sigma}_x = 0$. In this case, the value of the parameter λ is unknown $(\lambda \to \infty)$. Consequently, the appropriate threshold for the image denoising process cannot be determined. Therefore, the dissertation proposes that the threshold λ_1 defined in Equation (3.9) be reformulated as given in Equation (3.10).

$$\lambda_1 = \begin{cases} \beta \dfrac{\hat{\sigma}_w^2}{\hat{\sigma}_x}, & \text{if } \hat{\sigma}_y^2 > \hat{\sigma}_w^2 \\[2mm] \max\limits_{j,k=1,...,n} \{C_{j,k}\}, & \text{otherwise} \end{cases} \qquad (3.10)$$

Where: The scaling paramete β is determined according to the following equation

$$\beta = \sqrt{\log\left(\frac{L_k}{J}\right)} \quad (3.11).$$

The coefficient k in Equation (3.10) is assigned values of 2, 3, 4, 5, 6, and 10 to evaluate the denoising performance under different conditions.

- **Algorithm** Denoising crop images acquired by the Mobile Robot at sensor clusters in the agricultural greenhouse

Input: Original image: $g_{i,j}, \{i, j = 1, 2, ..., N\}$; Additive Noise: $\eta_{i,j}, \{i, j = 1, 2, ..., N\}$; Total number of multiscale decomposition levels of the image: J; Coefficient value: κ.

Output: Denoised image: $\hat{g}_{ij}, \{i, j = 1, 2, ..., N\}$;

1: Perform multiscale analysis of the Gaussian noise–corrupted image using the wavelet transform.

2: - Estimate the noise variance at the first decomposition level of the wavelet transform using the Equation (3.6).

3: At the subband level $k^{th}, \{k = 1, 2, ..., J\}$

- Compute the scaling parameter β using the Equation (3.11).

- Compute the standard deviation $\hat{\sigma}_x$ based on Equations (3.7) and (3.8).

- Compute threshold value λ_1 by Equation (3.10).

- Apply the threshold softening technique to the noise coefficients using Equation (3.2).

4: Perform the inverse multiresolution wavelet transform to reconstruct the denoised image $\hat{g}$

5: The algorithm terminates with the reconstructed image $\hat{g}$ when the condition $MSE(\hat{g}) = \frac{1}{N^2} \sum_{i,j=1}^{N} (\hat{g}_{ij} - g_{ij})^2$ is satisfied.

3.3 Proposing the enhancements of the YOLO model

YOLO is a deep neural network architecture designed for object detection by predicting bounding boxes and class probabilities directly from a single image in a single forward pass. Unlike two-stage detectors such as R-CNN and Faster R-CNN, YOLO performs classification and localization simultaneously, thereby achieving superior processing speed and making it highly suitable for real-time applications. YOLOv11 is an artificial intelligence model based on a convolutional neural network (CNN) architecture, as introduced by the authors in [20]. In the layer structure of the YOLOv11 model (Figure 3.4), the convolutional (Conv) layers are responsible for extracting salient features from the input data, with each layer organized as illustrated in Figure 3.5.

SiLU (Sigmoid-weighted Linear Unit): an activation function that has demonstrated notable effectiveness in function approximation within neural networks, particularly in reinforcement learning applications.

SiLU is computed by multiplying the input of a unit by the output of the sigmoid function applied to that input [22]:

$$\alpha_k(x) = x.\sigma(x) \tag{3.11}$$

Where, x denotes the input of the unit and $\sigma(x)$ denotes the sigmoid function. The sigmoid function is defined as follows:

$$\sigma(x) = \frac{1}{1 + e^{-x}} \tag{3.12}$$

However, the SiLU function exhibits limited adaptability to diverse data distributions, and its response mechanism when handling inputs with large absolute values remains constrained. On this basis, the dissertation proposes a modified SiLU function, referred to as the αSiLU function.
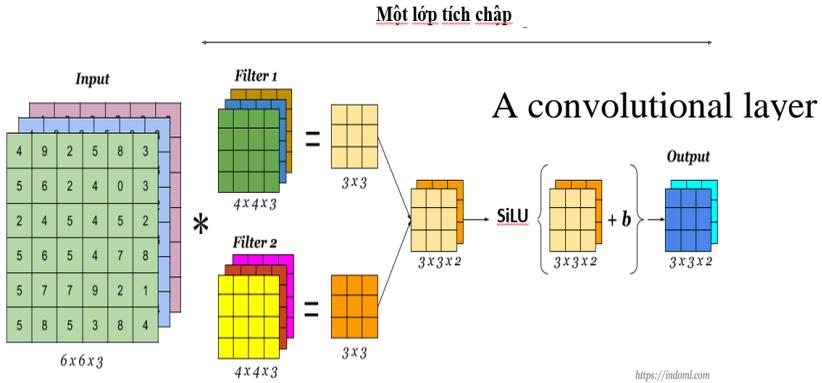
Figure 3.3 A fully connected layer with bias b and the SiLU activation function. [21]

• **Propose the αSiLU activation function**: is a variant of SiLU with a scaling parameter α, enabling adaptive adjustment of the gradient. The αSiLU function is defined as:

$$f(x) = x\alpha \frac{1}{1 + e^{-\alpha x}} = \alpha x . \text{sigmoid}(\alpha x) = \alpha x . \sigma(\alpha x) \tag{3.13}$$

The derivative of αSiLU activation function:

$$f'(x) = \alpha \frac{1}{1 + e^{-\alpha x}} + \alpha x \frac{\alpha e^{-\alpha x}}{(1 + e^{-\alpha x})^2}$$
$$= \alpha\,\sigma(\alpha x) + \alpha^2 x\,(\sigma(\alpha x) - \sigma^2(\alpha x))$$
$$= \alpha\,[f(x) + \sigma(\alpha x)(1 - f(x))] \tag{3.14}$$

Where, σ(x) denotes the sigmoid function, and α is a tunable parameter that controls the slope of the activation function.

3.4 Simulation and disscusion

3.4.1 Denoising agricultural crop images.

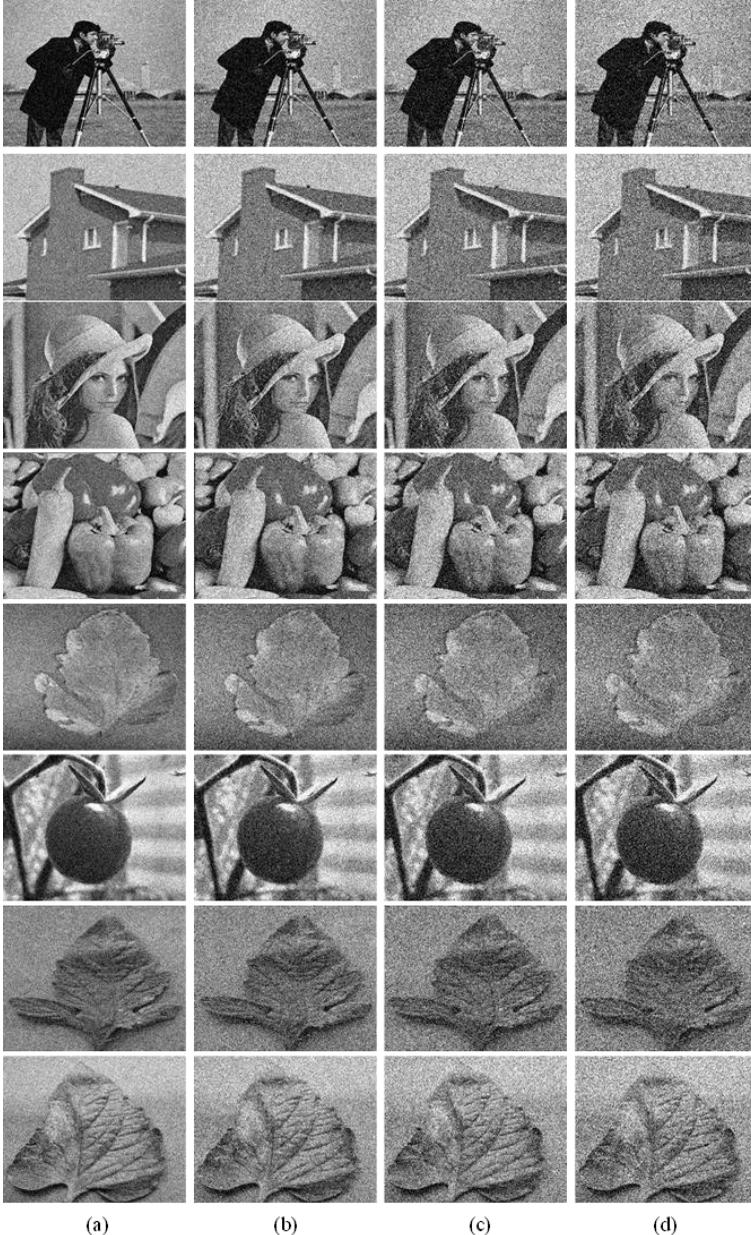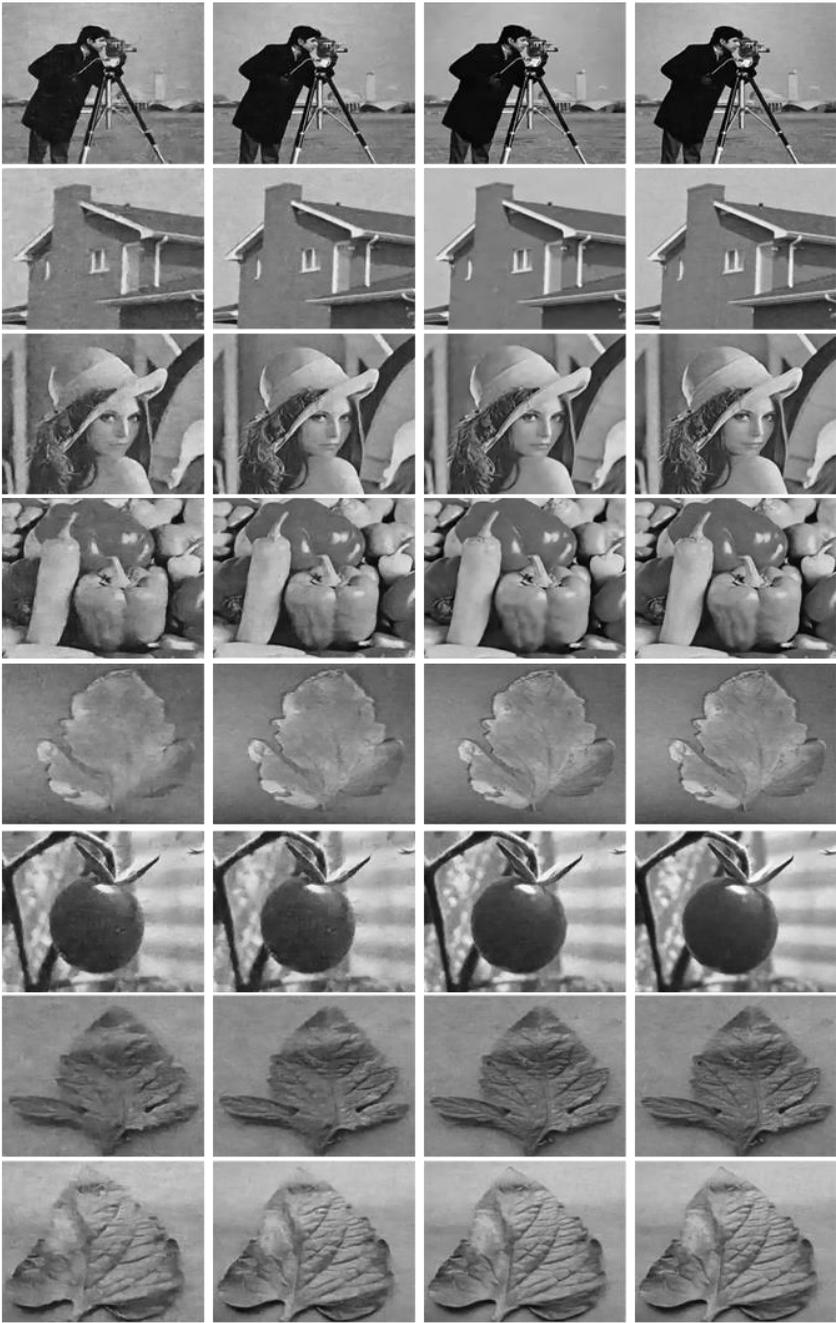*Figure* 3.4 Experimental images with different noise levels: (a) σ = 0,01, (b) 0,02, (c) 0,03 và (d) 0,04

Figure 3.5 Denoising results on the experimental images with a noise level σ = 0,01 using different methods.: (a) BS, (b) NS, (c) AI, (d) OP.

To comprehensively evaluate the proposed method, the following denoising techniques were employed for comparison in the experimental analysis: Bayes Shrink (BS), Normal Shrink (NS), the AI-based method (AI), and the proposed image denoising method (OP). The denoising results on the test images are illustrated in Figure 3.5.

In summary, the experimental simulation results demonstrate that the proposed OP algorithm achieves superior denoising performance, both subjectively in terms of visual quality and quantitatively based on PSNR values. In contrast, the BS and NS algorithms exhibit lower performance compared to the AI and OP methods, although their PSNR values remain within an acceptable range.

3.4.2 The Proposed improved YOLO model

• *Dataset*

Table 3.1: Dataset used in the simulation

No.	Crop species	The number of image	The crop disease	Data source
1	Tomato	16.075	Bacterial Spot, Early Blight, Late Blight, Leaf Mold, Yellow Leaf Curl Virus, Mosaic Virus, Septoria Leaf Spot and helathy leaves.	One dataset was collected under controlled conditions from [23], and the PlantDoc dataset was collected in field environments from [24].
2	Cucumber	7.920	Healthy cucumber leaves, Powdery mildew and Downy mildew leaves	Reference in study [25]

To ensure consistency with the input requirements of the YOLO model, all images were preprocessed and resized to 640×640 pixels. The aggregated dataset was then randomly divided into three subsets: training (80%), validation (10%), and testing (10%) to facilitate objective model evaluation.

* Evaluation methodology

Table 3.2: Model evaluation metrics

No.	Evaluation metrics	Mathematical formulation	Defination
1	*Precision (P)*	$P = \dfrac{TP}{TP + FP} * 100\%$	The ratio of correctly predicted bounding boxes to the total number of predicted bounding boxes, reflecting the model's ability to avoid false detections.
2	*Recall (R)*	$R = \dfrac{TP}{TP + FN} * 100\%$	The proportion of actual objects correctly detected by the model, indicating its sensitivity to missed detections.

No.	Evaluation metrics	Mathematical formulation	Defination
3	*F1-score*	$\text{F1-score} = 2 * \dfrac{P*R}{P+R} * 100\%$	The harmonic mean of Precision and Recall, providing a balanced measure, particularly useful in class-imbalanced scenarios.
4	*mAP@50 và mAP@50:95*	$\text{mAP} = \dfrac{\sum_{c=1}^{C} AP(c)}{C} * 100\%$	A composite metric reflecting detection accuracy across all object categories, computed by averaging the Average Precision (AP) values.

To evaluate the effectiveness of the proposed α-SiLU activation function within YOLO models, the dissertation employs several standard evaluation metrics commonly used in object detection tasks (Table 3.2).

- The model was trained on a hardware platform comprising an NVIDIA GeForce GTX 1660 GPU (6 GB VRAM), an Intel Xeon E5-2689 CPU, and 64 GB of RAM, operating on Windows 10. The software environment included Python 3.9.19, PyTorch 2.3.1 with CUDA 11.8 support, and Ultralytics 8.3.9.

The results of training model

a) Evaluation on the YOLOv11n model

The training results of the YOLOv11n model on the two plant disease datasets—tomato and cucumber—using the proposed activation function are presented in Tables 3.3 and 3.4.

Table 3.3: The training results on the tomato disease dataset

Model	Activation function	α	P (%)	R (%)	F1-score (%)	mAP@50 (%)	mAP@50-95 (%)
YOLOv11n	αSiLU	0,5	95,70	83,40	89,13	91,80	82,00
	αSiLU	0,7	95,20	**83,80**	89,14	91,80	81,70
	αSiLU	0,8	96,10	82,80	89,14	92,20	82,10
	αSiLU	0,9	94,80	84,10	89,13	92,00	**82,20**
	αSiLU	0,95	95,30	84,60	89,63	91,90	81,90
	SiLU	1	*95,20*	*83,40*	*88,91*	*91,30*	*81,30*
	αSiLU	1,025	**96,70**	83,60	89,67	91,70	81,60
	αSiLU	**1,05**	95,70	84,40	**89,70**	**92,40**	**82,00**
	αSiLU	1,055	95,30	83,50	89,01	91,70	81,70
	αSiLU	1,1	95,20	83,30	88,85	91,60	81,80
	αSiLU	1,5	94,40	84,60	89,23	91,30	81,30
	αSiLU	1,8	95,60	**83,80**	89,31	91,50	81,40
	αSiLU	2	96,30	83,40	89,39	91,60	81,50

Table 3.4: Training results on the cucumber disease dataset

Model	Activation function	α	P (%)	R (%)	F1-Score (%)	mAP@50 (%)	mAP@50–95 (%)
	αSiLU	0,5	87,40	87,50	87,45	94,20	80,70
	αSiLU	0,7	87,40	87,10	87,25	94,30	80,90
	αSiLU	0,85	87,10	87,30	87,20	94,10	80,60
	αSiLU	0,9	87,60	86,30	86,95	94,00	80,50
	αSiLU	0,95	89,10	85,90	87,47	94,20	80,70
	SiLU	1	87,80	87,00	87,40	94,10	80,80
YOLOv11n	αSiLU	1,025	88,00	86,00	86,99	94,10	80,60
	αSiLU	**1,05**	87,80	87,60	87,70	**94,30**	**81,00**
	αSiLU	1,06	88,00	87,30	87,65	94,20	80,80
	αSiLU	1,08	**89,60**	85,60	87,55	94,30	80,70
	αSiLU	1,1	88,40	86,30	87,34	94,20	80,70
	αSiLU	1,5	88,10	87,90	**88,00**	94,20	80,90
	αSiLU	1,8	86,60	**88,10**	87,34	93,90	80,80
	αSiLU	2	87,80	86,70	87,25	94,10	80,80

The experimental results indicate that ($\alpha = 1.05$) represents the optimal configuration, providing a clear improvement over the standard SiLU and maintaining stable performance across both datasets. Although ($\alpha = 0.9$) achieves the highest mAP@50–95, it lacks overall stability. Other values, such as 0.95 and 1.5, also yield competitive results, particularly on balanced datasets.

Overall, the range ($\alpha \in [0.95, 1.1]$) emerges as a practically optimal region, ensuring good generalization capability, gradient stability, and suitability for real-time models deployed on edge devices.

b) Experimental comparison among different YOLO versions

To further validate the generalization capability of the proposed αSiLU activation function, the dissertation extends the experimental evaluation to other YOLO variants, specifically YOLOv5n, YOLOv8n, and YOLOv10n.

Table 3.5: Performance evaluation of YOLO architectures on the cucumber disease dataset

Models	Precision	Recall	F1-score	mAP@50	mAP@50-95
YOLOv5n (SiLU)	88,10%	84,50%	86,26%	93,50%	79,30%
YOLOv5n (α = 1,05)	88,40%	85,00%	**86,67%**	**93,60%**	**79,30%**
YOLOv8n (SiLU)	85,70%	87,00%	86,35%	93,40%	79,70%
YOLOv8n (α = 1,05)	86,50%	87,20%	**86,85%**	**93,50%**	**79,80%**
YOLOv10n (SiLU)	88,80%	84,60%	86,65%	93,50%	79,40%
YOLOv10n (α = 1,05)	89,70%	84,90%	**87,23%**	**94,00%**	**79,80%**
YOLOv11n(SiLU)	87,80%	87,00%	87,40%	94,10%	80,80%
YOLOv11n (α = 1,05)	87,80%	87,60%	**87,70%**	**94,30%**	**81,00%**

Table 3.6: Performance evaluation of YOLO architectures on the tomato disease dataset

Models	Precision	Recall	F1-score	mAP@50	mAP@50-95
YOLOv5n (SiLU)	88,10%	84,50%	86,26%	93,50%	79,30%
YOLOv5n (α = 1,05)	88,40%	85,00%	**86,67%**	**93,60%**	**79,30%**
YOLOv8n (SiLU)	85,70%	87,00%	86,35%	93,40%	79,70%
YOLOv8n (α = 1,05)	86,50%	87,20%	**86,85%**	**93,50%**	**79,80%**
YOLOv10n (SiLU)	88,80%	84,60%	86,65%	93,50%	79,40%
YOLOv10n (α = 1,05)	89,70%	84,90%	**87,23%**	**94,00%**	**79,80%**
YOLOv11n(SiLU)	87,80%	87,00%	87,40%	94,10%	80,80%
YOLOv11n (α = 1,05)	87,80%	87,60%	**87,70%**	**94,30%**	**81,00%**

On the cucumber dataset (Table 3.5), integrating αSiLU ((\alpha = 1.05)) improves performance across all models, with YOLOv11n achieving the highest results at 94.3% mAP@50 and 81.0% mAP@50–95, outperforming the standard SiLU by +0.2%. On the tomato dataset (Table 3.6), which is characterized by class imbalance, αSiLU continues to deliver positive outcomes, particularly for YOLOv10n and YOLOv11n (up to +1.1% mAP@50 and +0.7% mAP@50–95), although YOLOv5n and YOLOv8n exhibit a slight decrease in Recall.

In summary, αSiLU proves to be an effective drop-in replacement activation function that requires no architectural modifications while delivering consistent performance improvements. It demonstrates strong scalability across multiple YOLO generations and is well suited for applications demanding both high detection accuracy and computational efficiency.

c) Experimental comparison among activation function

To gain deeper insight into the functional impact of αSiLU, the PhD candidate conducted a comparative analysis with several widely used activation functions, including LeakyReLU, ReLU, Mish, GELU, ELU, and the default SiLU. The results are presented in Tables 3.7 and 3.8.

Table 3.7: Evaluation of alternative activation functions on the tomato disease dataset

Models	Activation function	mAP@50 (%)	mAP@50-95 (%)	Latency (ms)
YOLOv11n	LeakyReLU	91,00	80,60	5,9
YOLOv11n	ReLU	91,2 0	80,80	5,8
YOLOv11n	Mish	91,20	81,30	5,9
YOLOv11n	GELU	91,40	81,30	5,9
YOLOv11n	ELU	91,70	81,60	5,9
YOLOv11n	SiLU	91,30	81,30	6,1
YOLOv11n	CAReLU	91,50	80,90	12,1
YOLOv11n (α = 1,05)	**αSiLU**	**92,40**	**82,00**	6,6

Table 3.8: Evaluation of alternative activation functions on the cucumber disease dataset

Models	Activation function	mAP@50 (%)	mAP@50-95 (%)	Latency (ms)
YOLOv11n	LeakyReLU	94,00	80,10	6,4
YOLOv11n	ReLU	94,20	80,20	6,3
YOLOv11n	Mish	94,10	80,80	6,2
YOLOv11n	GELU	94,20	80,70	6,4
YOLOv11n	ELU	94,10	80,60	6,3
YOLOv11n	SiLU	94,10	80,80	6,6
YOLOv11n	CAReLU	93,80	80,10	12,4
YOLOv11n ($\alpha = 1,05$)	**αSiLU**	**94,30**	**81,00**	7,0

Overall, αSiLU outperforms the other activation functions in detection accuracy on both datasets while maintaining significantly lower computational cost. These findings further confirm the effectiveness of αSiLU, not only as a direct replacement for SiLU but also as a practical and efficient alternative to more complex activation functions such as Mish, GELU, and CAReLU.

3.6 The conclusion of chapter 3

Chapter 3 has accomplished several key objectives of the dissertation as follows:

• Investigated and proposed an image denoising method for crop image datasets acquired by a mobile robot from vision sensors deployed at various locations within the monitored area. The collected data were transmitted to the control center for analysis and supervisory control of crop growth, with particular emphasis on plant disease detection.

• Proposed an improved YOLO-based model for plant disease detection by refining the SiLU activation function through the introduction of a scaling coefficient (α). The αSiLU activation function enhances the model's nonlinear representation capability, accelerates convergence during training, and improves detection accuracy compared to several other activation functions. Preliminary experimental results indicate that the improved model achieves superior disease detection performance, meeting practical application requirements under greenhouse conditions. The research findings presented in this chapter have been published in Publication No. 5 of the PhD candidate.

CONCLUSIONS AND RECOMMENDATIONS

The dissertation has achieved its stated objectives, namely: enabling mobile robot navigation in agricultural greenhouses to ensure complete data acquisition from cluster-head sensor nodes within a predefined allowable time frame, while prioritizing the reduction of energy consumption for sensor clusters. Furthermore, the system supports monitoring crop growth in greenhouse environments and facilitates timely detection of plant diseases, thereby enabling appropriate intervention measures to improve overall yield. In addition, the dissertation conducted simulations and performance evaluations of the proposed algorithms and the improved model. The main contributions of the dissertation are summarized as follows:

➢ **The dissertation proposes a navigation solution for a mobile robot to collect complete data from a wireless sensor network within a predefined allowable time horizon.** The proposed solution is designed to satisfy the following requirements: (i) minimize the total travel distance of the mobile robot; (ii) ensure that each cluster-head sensor node is visited within the reporting deadline (ξ_0), thereby preventing data overflow at any cluster-head node; and (iii) guarantee that the mobile robot completes its dedicated trajectory within the specified reporting period (ξ_0). The proposed solution supports environmental monitoring and crop growth supervision in agricultural applications.

➢ **The dissertation proposes an enhanced YOLO-based model to improve plant disease detection performance in agricultural greenhouses.** The improved YOLO model is developed by introducing the proposed αSiLU activation function. This activation function improves mAP@50–95, a metric that is particularly critical in agricultural image diagnosis, where disease symptoms are often diverse and difficult to recognize. The study identifies an optimal range of (α) that balances representational capacity and gradient flow while maintaining high mAP and F1 scores. This convergence indicates that αSiLU offers task-adaptive flexibility without requiring architectural modifications. Overall, the proposed approach enhances the effectiveness of crop growth monitoring in agricultural settings.

➢ **Future Research Directions:**

In subsequent research, the PhD candidate will focus on investigating navigation strategies for a multi-mobile-robot system to collect sensor data from wireless sensor networks deployed in real-world agricultural greenhouses, thereby evaluating practical applicability. Additionally, future work will assess the performance of the improved SiLU activation function on the latest versions of artificial intelligence models and across diverse plant disease datasets.

LIST OF THE PUBLICATIONS RELATED TO THE DISSERTATION

1. "Xây dựng hệ định vị, bản đồ hóa cho robot tự hành trong nhà kính nông nghiệp dựa trên hệ điều hành lập trình cho robot" *Tạp chí KH&CN quân sự, Số Đặc san Hội thảo Quốc gia FEE*, 10/2021, tr.168-175, ISSN: 1859-1043.

2. "Xây dựng hệ điều hướng trên bản đồ, định vị SLAM cho Robot tự hành trong nhà kính nông nghiệp dựa trên hệ điều hành ROS" *Proceedings the 6th Vietnam International Conference and Exhibition on Control and Automation VCCA-2021*, ISBN 978-604-73-5569-3.

3. "Lập quỹ đạo cục bộ dựa trên bản đồ đồng thời SLAM cho Robot tự hành trong nhà kính nông nghiệp trên nền tảng hệ điều hành ROS" *Hội thảo quốc gia lần thứ XXIV: Một số vấn đề chọn lọc của công nghệ thông tin và truyền thông*- Thái Nguyên, 13-14/12/2021.

4. "Enhancing network lifetime and data integrity in WSNs via optimized mobile robot trajectories" *Journal of Robotics and Control (JRC)* 2025, 6(5), pp. 2260-2271, Scopus indexed (Q2).

5. "Improving YOLO-based Plant Disease Detection using αSILU: a Novel Activation Function for Smart Agriculture" *AgriEngineering* 2025, 7(9), 271,
   JCR - Q2 (Agricultural Engineering).

6. "Appication of Fast Segment Anything Model (FASTSAM) for autonomous robot indentifying plant diease" *Thanh Dong University Journal of Sciences and Technology*, 2023 Sep, pp.50, ISSN 2734-9500.

7. "Xây dựng hệ điều hướng cho Robot tự hành giám sát sâu bệnh trên cây trồng trong nhà lưới dựa trên hệ điều hành ROS", *Proceedings the 7th Vietnam International Conference and Exhibition on Control and Automation VCCA-2024*, ISBN 978-604-937-357-2.